AIP | Advances

Crystallographic changes in lead zirconate titanate due to neutron irradiation

Alexandra Henriques, Joseph T. Graham, Sheldon Landsberger, Jon F. Ihlefeld, Geoff L. Brennecka, Donald W. Brown, Jennifer S. Forrester, and Jacob L. Jones

---

Articles you may be interested in

Neutron irradiation effects on domain wall mobility and reversibility in lead zirconate titanate thin films
J. Appl. Phys. **113**, 124104 (2013); 10.1063/1.4795869

Influence of crystal phases on electro-optic properties of epitaxially grown lanthanum-modified lead zirconate titanate films
Appl. Phys. Lett. **96**, 072901 (2010); 10.1063/1.3308506

Nonlinearity and fatigue in ferroelectric lead zirconate titanate
J. Appl. Phys. **100**, 054109 (2006); 10.1063/1.2337389

Heterolayered lead zirconate titanate thin films of giant polarization
J. Appl. Phys. **96**, 5706 (2004); 10.1063/1.1803921

Photoinduced poling of lead titanate zirconate thin films
Appl. Phys. Lett. **71**, 2854 (1997); 10.1063/1.120154

Crystallographic changes in lead zirconate titanate due to neutron irradiation

Alexandra Henriques,[1] Joseph T. Graham,[2] Sheldon Landsberger,[3] Jon F. Ihlefeld,[4] Geoff L. Brennecka,[4] Donald W. Brown,[5] Jennifer S. Forrester,[6] and Jacob L. Jones[6,a]

[1]*Department of Materials Science and Engineering, University of Florida, Gainesville, Florida 32611, USA*
[2]*Department of Materials Science and Engineering, University of Tennessee, Knoxville, Tennessee 37996, USA*
[3]*Nuclear Engineering Teaching Lab, Department of Mechanical Engineering, University of Texas, Austin, Texas 78712, USA*
[4]*Electronic, Optical, and Nanomaterials Department, Sandia National Laboratories, Albuquerque, New Mexico 87185, USA*
[5]*Los Alamos Neutron Science Center, Los Alamos, New Mexico 87185, USA*
[6]*Department of Materials Science and Engineering, North Carolina State University, Raleigh, North Carolina 27695, USA*

Piezoelectric and ferroelectric materials are useful as the active element in non-destructive monitoring devices for high-radiation areas. Here, crystallographic structural refinement (*i.e.*, the Rietveld method) is used to quantify the type and extent of structural changes in $PbZr_{0.5}Ti_{0.5}O_3$ after exposure to a 1 MeV equivalent neutron fluence of 1.7×10^{15} neutrons/cm^2. The results show a measurable decrease in the occupancy of Pb and O due to irradiation, with O vacancies in the tetragonal phase being created preferentially on one of the two O sites. The results demonstrate a method by which the effects of radiation on crystallographic structure may be investigated. © *2014 Author(s). All article content, except where otherwise noted, is licensed under a Creative Commons Attribution 3.0 Unported License.* [http://dx.doi.org/10.1063/1.4902179]

Many sensor and electronic devices are used in high radiation areas.[1–7] Ferroelectric materials are useful in these devices because of their ability to interact with the environment and store information, *e.g.*, as electromechanical sensors and nonvolatile memories.[8] $Pb(Zr_xTi_{1-x})O_3$ (PZT) is a widely used ferroelectric/piezoelectric material because it has high electromechanical coupling, in particular at compositions near the morphotropic phase boundary (MPB).[9] The electromechanical coupling of PZT is also highly dependent on the interaction of ferroelastic domain walls and point defects, the latter of which are generally known to be affected by irradiation.[9,10] While several studies have shown that irradiation, in particular with neutrons, causes irreversible changes to the electromechanical properties of ferroelectric materials, there is little empirically known about the type and concentration of point defects and other structural changes created during irradiation.[11–15] For example, Miclea *et al*. found that the planar electromechanical coupling factor, k_p, decreased after exposure to ~1×10^{15} neutrons/cm^2 and degraded more substantially with increased exposure.[11] Miclea *et al*. also noted an increase in unit cell volume and a decrease in lattice aspect ratio (c/a) with neutron irradiation,[11] a result that was in agreement with Toacsan *et al*.[12] The structural changes were hypothesized to result from an increased concentration of oxygen vacancies, though no direct measure of vacancy concentration was available.

Diffraction is a useful tool through which to characterize the effects of irradiation on materials' structure. In particular, the diffracted intensities are a function of the scattering factor of the elements and their occupancies, meaning that site occupancies can be determined from the diffraction pattern.

---

[a]Author to whom correspondence should be addressed. Electronic mail: jacobjones@ncsu.edu. Tel: 919-515-4557.

4, 117125-1

Crystallographic refinement (*i.e.*, the Rietveld method) is one analysis technique that can be used to model the diffraction patterns, providing quantitative information about the lattice parameters, strain and other microstructural information, as well as the occupancies of different lattice sites.[16] Site occupancies provide a direct link to the changing point defect concentrations that are expected with irradiation. Lattice parameters provide an indirect and secondary measurement of such effects. Thus, crystallographic refinement using diffraction patterns is a potentially useful approach to characterize the type and concentration of point defects in irradiated materials.

Polycrystalline PZT powders with a composition of $x=0.5$ ($PbZr_{0.5}Ti_{0.5}O_3$) were investigated in the present work. This composition was selected in order to avoid the complexity of the monoclinic phase of PZT that is sometimes reported at a composition of $PbZr_{0.52}Ti_{0.48}O_3$, though near enough to the MPB to be technologically relevant due to useful electromechanical coupling. Compositions near the MPB can contain single phase polymorphs (*e.g.*, tetragonal structure of space group *P4mm*) or co-existing phases (*e.g.*, tetragonal *P4mm* co-existing with a rhombohedral space group *R3m*). Samples were synthesized in two reaction steps using solid state synthesis from starting powders of PbO (99.9% purity, Alfa Aesar), TiO_2 (99.85% purity, Alfa Aesar), and ZrO_2 (99.5% purity, Alfa Aesar). The two reaction step approach is similar to that used by Swartz and Shrout to synthesize $Pb(Mg_{1/3}Nb_{2/3})O_3$.[17] This type of processing is generally used to maximize *B*-site homogeneity. The ZrO_2 and TiO_2 powders were ground for 10 min, ball-milled in ethanol with yttria-stabilized zirconia media for 12 h, then dried and sieved to less than 200 μm. The powder was calcined at 1300°C for 4 h in a closed alumina crucible using a heating rate of 4°C/min. The PbO was then added in an amount containing 2 wt% excess of what is stoichiometrically required (to compensate for volatility) and the powder was ground for an additional 10 min. The powder was ball-milled again for 12 h, dried, and sieved to less than 200 μm. The solid state reaction was carried out with the sample as a powder, using a ramp rate of 4°C/min, and held at 950°C for 3 h. Half of the synthesized powder was irradiated and half was aged an equivalent length of time at ambient conditions as a control.

Irradiation of samples was carried out at the University of Texas - Austin, on a 1 MW TRIGA Mark II nuclear research reactor capable of producing a 1 MeV equivalent neutron flux of 2.4×10^{12} cm^{-2} s^{-1} at full power. The 1 MeV equivalent flux is determined with reference to a Si displacement Kerma. The powder was exposed to a nominal 1 MeV equivalent fluence of 1.7×10^{15} neutrons/cm^2 over 1 h. This fluence is in a conventional range relevant to radiation effects in electronics (which are extremely sensitive to radiation). The samples were irradiated within a Cd filter, allowing for irradiation of the samples with a harder spectrum that results in almost the same damage with less activation of the PZT. This correspondingly limits the decay time from months to days. Approximately 10 g of PZT powder was loaded into a Rotary Specimen Rack (RSR), a 40-sample vial annular ring, which orbits the core fuel assembly. The flux in the RSR is essentially isotropic and its time average is uniform across vial locations.

In the neutron environment, the nuclei in the sample powders undergo a number of neutron-nuclide interactions. Elastic and inelastic scattering collisions result in the creation of primary knock-on atoms and, ultimately, displacement damage cascades producing structural defects. Radiative capture – the absorption of a neutron and emission of a de-excitation gamma ray – is the dominant mechanism responsible for transmutation of the elements in the thermal neutron environment. Transmutation mainly results in the production of Bi, Mo and F isotopes. Neutron activation calculations reveal, however, that the concentration of these elements is below 5×10^{-10} atomic fraction – well below the concentration of radiation induced defects and initial impurities present in the sample powders. Threshold absorption reactions occurring with fast neutrons can produce a wider array of transmuted species as well as light elements such as H and He. The production rates for these products are considerably lower than the rates from radiative capture and, therefore, deemed insignificant.

Time-of-flight neutron diffraction patterns of the control and irradiated powders were recorded at room temperature using the Spectrometer for Materials Research at Temperature and Stress (SMARTS) instrument at the Los Alamos Neutron Science Center (LANSCE). The slow neutron damage from the scattering measurements (~1x10^7 cm^{-2}/s thermal neutron flux) was insignificant when compared to the very fast neutron damage from the irradiation (*i.e.*, several orders of magnitude lower). There is sometimes minor damage from neutron activation induced decay recoil, but it is generally small compared to the damage received from elastic scattering of fast neutrons. A detailed

description of the SMARTS instrument is given in Brown *et al.*[18] The pulsed neutron source at LAN-SCE enables the use of the time-of-flight technique where full diffraction patterns (from 0.4 to 3.8 Å) are recorded in each of the two detector banks. The wavelength dependent resolution at 90° is ~0.4%. The samples were loaded into 9.5 mm diameter by 15 mm high vanadium cans, which were positioned centrally in the 5 mm wide neutron beam. The patterns were recorded for ~3.6 μAmp h for the control sample and ~11 μAmp h for the irradiated sample, the latter being longer because additional measurement time was available and therefore used to improve counting statistics.

Crystal structure refinements of the diffraction data were carried out using the Rietveld refinement program GSAS.[19] The background was modeled using 12 parameters in function type 6, a power series model that accounts for the background typically recorded using the SMARTS diffractometer. Refined values from a CaF_2 instrument standard allowed the diffractometer constants DIFA and DIFC to be set at 5.06 and 12998 respectively, and not refined. These constants relate the time of flight, t, of a reflection to its d-spacing, d. In addition, within profile function 3, profile parameters alp-0 (0.06403), bet-0 (0.02586), and bet-1 (0.009396) were set, and not refined, as these parameters are governed by the moderator. Two phases were used in a mixed-phase refinement to model the data: a tetragonal phase of space group *P4mm* (illustrated in Fig. 1(a)), and a rhombohedral phase of space group *R3m* (illustrated in Fig. 1(b)). In the present work, the reflections and profiles are labeled according to their pseudo-cubic (pc) indices. Inspection of the $\{200\}_{pc}$ profile indicates that the combination of *P4mm* and *R3m* is necessary to model the diffraction patterns. In the initial composition of $PbZr_{0.5}Ti_{0.5}O_3$, a single phase tetragonal phase may be expected based on known phase diagrams. However, studies have shown varied phase assemblages and local heterogeneities in the region of the MPB in PZT (*e.g.* Refs. 20–22) and only small changes in local stoichiometry are required to induce two phases. Parameters refined included the 2θ zero offset, scale factor, lattice parameters, atomic positions, atomic displacement parameters, and atomic site occupancies. The atomic position and displacement parameters of Zr and Ti were constrained to be equal as they share the *B*-site, and the site occupancies were constrained to equal a total of 1 (*i.e.*, fully occupied), and refined opposite to each other. The peak shape parameters from profile function 1 that can be refined were constrained to equal each other between the two phases, and these parameters were refined independently and then in combination. The refinement outputs and quality of fit indicators are listed in Table I.

Figure 2 presents the simulated and measured diffraction patterns for the two crystallographic refinements. The control sample is presented in Fig. 2(a), with additional views of the $\{110\}_{pc}$, the $\{111\}_{pc}$, and the $\{200\}_{pc}$ profiles. Figure 2(b) shows the equivalent patterns for the irradiated sample. There are several aspects of the neutron patterns and models that are readily apparent. Firstly, the $\{110\}_{pc}$ profile is asymmetric, which is a result of several contributing reflections from the various phases. The atomic positions, which affect the relative intensities of the contributing reflections, were found to contribute to this profile asymmetry. The refinement outputs in Table I show that the 2nd oxygen (O(2)) displaces in a direction opposite (anti-parallel) to the *B*-site (Zr, Ti) displacement, a displacement mode that was necessary to fit the $\{110\}_{pc}$ profile. A wide variety of oxygen displacement modes have been observed in refined crystal structures of PZT, $BaTiO_3$, and $PbTiO_3$: the positions of the two independent oxygen atoms (identified as O(1) and O(2) in Fig. 1(a)) have been shown to vary in their displacement directions relative to the displacement of the *B*-site and with respect to each other.[23–25]
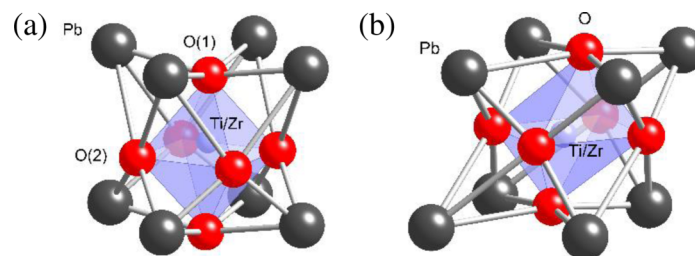

FIG. 1. Crystallographic structure of PZT in (a) the tetragonal *P4mm* space group. Unique lattice sites are indicated: Pb, Ti/Zr, O(1), and O(2), and (b) the rhombohedral *R3m* space group. Unique lattice sites are indicated: Pb, Ti/Zr, and O.

TABLE I. Crystallographic structure parameters from the refinements of the control and irradiated PZT. Values in parentheses reflect the estimated standard deviation of the last value, calculated in the refinement.

| Control PZT (Aged) Tetragonal ($P4mm$)					Irradiated PZT Tetragonal ($P4mm$)				
a (Å)	c (Å)	Cell volume (Å)^3	c/a	Profile fit	a (Å)	c (Å)	Cell volume (Å)^3	c/a	Profile fit
4.0383(2)	4.12764(3)	67.313(6)	1.0221(2)	R_p 1.34% R_{wp} 1.70% Chi^2 2.23	4.0385(2)	4.1298(2)	67.355(5)	1.0225(7)	R_p 1.15% R_{wp} 1.50% Chi^2 5.41
Site Positions					Site Positions				
	x	y	z	Occ.		x	y	z	Occ.
Pb	0.0	0.0	0.0	0.968(7)	Pb	0.0	0.0	0.0	0.911(2)
Zr	0.5	0.5	0.453(2)	0.511(2)	Zr	0.5	0.5	0.446(1)	0.459(6)
Ti	0.5	0.5	0.453(2)	0.489(2)	Ti	0.5	0.5	0.446(1)	0.541(6)
O1	0.5	0.5	-0.075(1)	1.002(7)	O1	0.5	0.5	-0.0819(9)	0.961(9)
O2	0.5	0.0	0.3961(9)	1.00(1)	O2	0.5	0.0	0.3941(6)	1.014(8)
Rhombohedral ($R3m$)					Rhombohedral ($R3m$)				
a (Å)	α (°)	Cell volume (Å)^3		Phase fraction (%)	a (Å)	α (°)	Cell volume (Å)^3		Phase fraction (%)
4.0855(5)	89.46(2)	68.18(2)		13.634(4)	4.0821(4)	89.44(1)	68.01(1)		17.005(2)
Site Positions					Site Positions				
	x	y	z	Occ.		x	y	z	Occ.
Pb	0.0	0.0	0.0	0.90(4)	Pb	0.0	0.0	0.0	0.84(5)
Zr	0.625(5)	0.625(5)	0.625(5)	0.5028(2)	Zr	0.653(7)	0.653(7)	0.653(7)	0.54(8)
Ti	0.625(5)	0.625(5)	0.625(5)	0.4972(2)	Ti	0.653(7)	0.653(7)	0.653(7)	0.46(8)
O1	0.582(2)	0.582(2)	0.047(4)	1.09(7)	O1	0.578(3)	0.578(3)	0.046(4)	1.09(9)
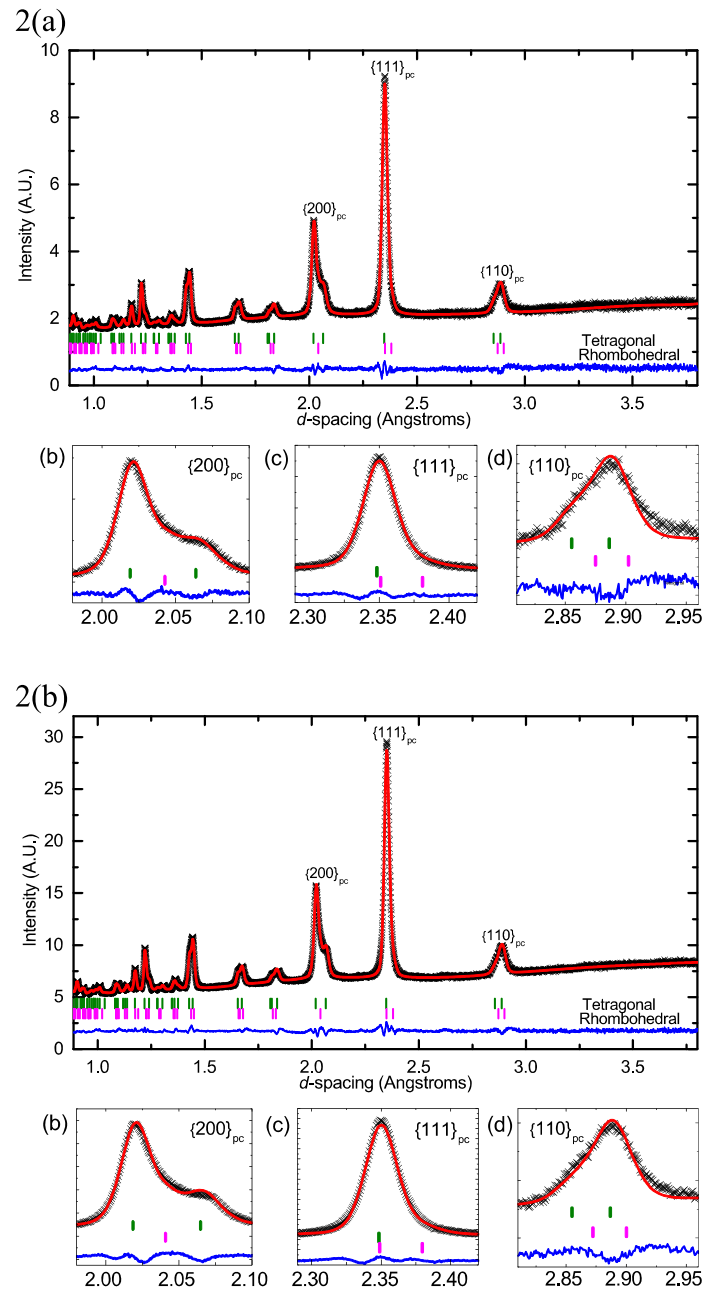
FIG. 2. Measured and modeled diffraction patterns for the control (a) and irradiated (b) samples. Insets in each pattern show the profiles of the pseudo-cubic {200}, {111}, and {110} profiles.

It can also be observed in Fig. 2 that the {111}$_{pc}$ profiles are well-modeled in these refinements. In contrast, the {200}$_{pc}$ profile was more difficult to model. Twin-related domain wall diffuse scattering is commonly observed in the {200}$_{pc}$ profiles of tetragonal ferroelectric diffraction patterns,[26,27] and this additional scattering affects the ability to adequately model these reflections in Rietveld refinement programs. Nevertheless, the two-phase *P4mm* + *R3m* model provides for reasonable fits to the diffraction data.

The refinement outputs shown in Table I provide a means to quantitatively compare the structures of the irradiated and control samples. The unit cell volume is one possible indicator of a structural

change that may occur with irradiation. In the present work, the unit cell of the tetragonal phase increases in volume by 0.062% with irradiation, while the unit cell volume of the rhombohedral phase decreases by 0.25%. Both of these changes are significantly smaller than the increase observed in Toacsan *et al.*[12] (~0.6%) after exposure at the highest radiation levels of 10^{17} neutrons/cm^2 (two orders of magnitude higher radiation levels than in the present work). The change in lattice aspect ratio of the tetragonal phase (c/a) in the present work (+0.05%) is also small relative to the change seen in Toacsan *et al.*[12] of -0.34%. The changes in unit cell volume and lattice aspect ratio with irradiation are therefore not deemed as significant under the conditions utilized in the present work.

Table I also reports the occupancies of all sites in the unit cell, some of which show consistent and significant changes. In particular, the Pb occupancy decreases consistently in both phases, in the tetragonal phase reducing from 0.968(7) to 0.911(2) (-5.7%) and in the rhombohedral phase from 0.90(4) to 0.84(5) (-6%). It is likely that the Pb or PbO accumulates at crystal surfaces (i.e. grain boundaries), dislocations, etc. The occupancy of O(1) in the tetragonal phase also decreases from 1.002(7) to 0.961(9) (-4.1%), while the occupancy of O(2) does not change significantly, indicating a preference for O(1) site vacancies over O(2) site vacancies. Modeling by Park and Chadi[28] suggested that O vacancies are more likely to occur parallel to the polarization direction (c-axis) in PbTiO$_3$ (*i.e.*, O(1) vacancies are more energetically favorable than the O(2) in the a/b-plane).[28] The results in the present work are consistent with this model, showing experimentally that oxygen vacancies preferentially occur on the O(1) site due to irradiation. Moreover, the results as a whole demonstrate that the Pb and O(1) sites are susceptible to displacement due to neutron irradiation.

The results in Table I also indicate some measurable differences in the Zr:Ti ratio of the tetragonal and rhombohedral phases between the control and irradiated samples. In the control sample, the Zr:Ti ratios in the tetragonal and rhombohedral phases are approximately 51:49 and 50:50, demonstrating close internal consistency between the two phases. After irradiation, the Zr:Ti ratio in the tetragonal phase decreases to approximately 46:54, whereas the ratio in the rhombohedral phase increases to approximately 54:46. These results may indicate an inclination towards phase separation during irradiation, a phenomena observed in other materials under sufficient irradiation, *e.g.* as shown in oxide glasses in Ref. 29.

The structural changes described above may relate to the irreversible changes in ferroelectric behavior and electromechanical properties that have been observed previously after neutron irradiation.[11–15] Microscopically, it has been suggested that defect dipoles play a significant role in domain wall pinning and that the concentration of defect dipoles can be altered irreversibly through neutron irradiation.[15] The present work shows measurable decreases in Pb and O occupancies, meaning that the vacancies created on these lattice sites during neutron irradiation likely play a role in domain wall pinning and irreversible changes to properties. The Pb and O defects may affect domain wall pinning directly or through incorporation into defect complexes containing more than one point defect. Nevertheless, the present work identifies these two sites as being affected by neutron irradiation and therefore likely playing a role in pinning of domain walls by point defects. It is also likely that chemical heterogeneity, as measured in the changing Zr:Ti ratio, may also influence electromechanical properties, perhaps through its effect on domain wall and interphase boundary motion.

In summary, changes in the crystallographic structure were determined in PZT after irradiation by neutrons. Analysis of diffraction patterns was undertaken using the Rietveld method and a two-phase structural model. The change in lattice aspect ratio (c/a) and unit cell volume of PZT showed minor changes relative to that observed after exposure to more extreme conditions in prior work. Under the moderate exposure levels explored in the present work, quantifiable and significant changes in Pb and O occupancies are observed, which indicate an increase in Pb and O vacancies as a result of neutron irradiation. A preference for oxygen vacancies was also noted on the O(1) site relative to the O(2) site, in agreement with prior theoretical results. A notable change in Zr:Ti ratio also resulted from irradiation. The results of the present work suggest that Pb and O(1) site vacancies likely play a role in domain wall pinning and the property changes that are observed in ferroelectric materials due to neutron irradiation.

[1] J. Bogaerts, B. Dierickx, G. Meynants, and D. Uwaerts, IEEE Trans. Electron Dev. **50**, 84 (2003).
[2] T. Calin, M. Nicolaidis, and R. Velazco, IEEE Trans. Nucl. Sci. **43**, 2874 (1996).
[3] P. E. Dodd and L. W. Massengill, IEEE Trans. Nucl. Sci. **50**, 583 (2003).
[4] P. E. Dodd, J. R. Schwank, M. R. Shaneyfelt, V. Ferlet-Cavrois, P. Paillet, J. Baggio, G. L. Hash, J. A. Felix, K. Hirose, and H. Saito, IEEE Trans. Nucl. Sci. **54**, 889 (2007).
[5] H. L. Hughes and J. M. Benedetto, IEEE Trans. Nucl. Sci. **50**, 500 (2003).
[6] A. H. Johnston, IEEE Trans. Nucl. Sci. **45**, 1339 (1998).
[7] J. D. Maimon, K. K. Hunt, L. Burcin, and J. Rodgers, IEEE Trans. Nucl. Sci. **50**, 1878 (2003).
[8] J. Rho, S. J. Kim, W. Heo, N.-E. Lee, H.-S. Lee, and J.-H. Ahn, IEEE Electron. Device Letters **31**, 1017 (2010).
[9] G. H. Haertling, J. Am. Ceram. Soc. **82**(4), 797 (1999).
[10] W. Zhu, I. Fujii, W. Ren, and S. Trolier-McKinstry, J. Am. Ceram. Soc. **95**, 2906 (2012).
[11] C. Miclea, C. Tanasoiu, C. F. Miclea, I. Spanulescu, and M. Cioangher, J. Phys. IV France **128**, 115 (2005).
[12] M. I. Toacsan, A. Ioachim, L. Nedelcu, and H. V. Alexandru, Prog. Solid State Chem. **35**, 531 (2007).
[13] R. A. Moore, J. M. Benedetto, J. M. McGarrity, and F. B. McLean, IEEE Trans. Nucl. Sci. **38**, 1078 (1991).
[14] C. Verbeck and P. Gaucher, Radiation and its Effects on Components and Systems – RADECS **93**, 166 (1993).
[15] J. T. Graham, G. L. Brennecka, P. Ferreira, L. Small, D. Duquette, C. Apblett, S. Landsberger, and J. F. Ihlefeld, J. Appl. Phys. **113**, 124104 (2013).
[16] R. A. Young, "The Rietveld Method," in *International Union of Crystallography*, edited by R. A. Young (Oxford University Press, Oxford, 1993).
[17] S. L. Swartz and T. R. Shrout, Mater. Res. Bull. **17**, 1245 (1982).
[18] D. W. Brown, S. R. Agnew, M. A. M. Bourke, T. M. Holden, S. C. Vogel, and C. N. Tome, Mater. Sci. Eng. A **399**, 1 (2005).
[19] A. C. Larson and R. B. Von Dreele, *General Structure Analysis System (GSAS), Los Alamos National Laboratory Report LAUR 86-748* (2004).
[20] A. M. Glazer, P. A. Thomas, K. Z. Baba-Kishi, G. K. H. Pang, and C. W. Tai, Phys. Rev. B **70**, 184123 9pp. (2004).
[21] R. Schierholz and H. Fuess, Phys. Rev. B **84**(6), 064122 12pp. (2011).
[22] R. Kirchhofer, D. R. Diercks, B. P. Gorman, J. F. Ihlefeld, P. G. Kotula, C. T. Shelton, and G. L. Brennecka, J. Am. Ceram. Soc., in press (2014).
[23] R. H. Buttner and E. N. Maslen, Acta. Cryst. B **48**, 764 (1992).
[24] C. J. Xiao, c. Q. Jin, and X. H. Wang, Mater. Chem. Phys. **111**, 209 (2008).
[25] A. M. Glazer and S. A. Mabud, Acta Cryst. B **34**, 1065 (1978).
[26] C. N. W. Darlington and R. J. Cernik, J. Phys.: condens. matter **3**, 4555 (1991).
[27] J. E. Daniels, J. L. Jones, and T. R. Finlayson, J. Phys. D: Appl. Phys. **39**, 5294 (2006).
[28] C. H. Park and D. J. Chadi, Phys. Rev. B **57**, R13961 (1998).
[29] K. Sun, L. M. Wang, R. C. Ewing, and W. J. Weber, Nucl. Instrum. Meth. B **218**, 368 (2004).